Simplified Numerical Modeling of Axially Loaded Circular Concrete-Filled Steel Stub Columns

Utsab Katwal, S.M.ASCE[1]; Zhong Tao, M.ASCE[2]; Md Kamrul Hassan, A.M.ASCE[3]; and Wen-Da Wang[4]

Abstract: Behavior of concrete-filled steel tubular (CFST) columns can be predicted accurately using detailed finite-element (FE) modeling, but such models are tedious to build and impractical for frame analysis. In contrast, computationally efficient fiber beam element (FBE) models can achieve the balance between accuracy and simplicity, and can be utilized for advanced analysis of structural systems. In FBE models, however, the material models themselves have to account for the interaction between the steel tube and core concrete. Therefore the accuracy of a FBE model depends mainly on the input material models. Although there are a few FBE models available in the literature for CFST columns, these models may not be suitable for some cases, especially when considering the rapid development and application of high-strength materials and/or thin-walled steel tubes. This paper proposes versatile, computationally simple, yet accurate steel and concrete models based on detailed FE modeling results of circular CFST stub columns under axial compression. The material models are then implemented in FBE modeling and the prediction accuracy is verified with a wide range of test data. **DOI: 10.1061/(ASCE)ST.1943-541X.0001897.**

Author keywords: Concrete-filled steel tubes; Confined concrete; Finite element modeling; Fiber beam model; Simplified simulation; Metal and composite structures.

Introduction

Steel-concrete composite structures consisting of concrete-filled steel tubular (CFST) columns have been widely used in modern construction because they offer many structural and economic benefits (Han et al. 2014a). Detailed three-dimensional (3D) finite-element (FE) models can be developed to precisely predict the behavior of composite structures, but such models are tedious to build and impractical for the analysis of large structural systems or for routine design. This is mainly due to the complexity in modeling, convergence issues, and long computational time. In this context, to achieve the balance between efficiency and accuracy in simulating CFST columns, fiber beam element (FBE) models can be utilized because of their simplicity in simulation and high computational efficiency. The FBE models are suitable for use in advanced analysis of composite frames. However, the main challenge is in developing proper material models which themselves have to account for the interaction between the steel tube and core concrete.

There are a few steel and concrete stress–strain ($\sigma-\varepsilon$) models available in the literature developed for FBE modeling of circular CFST columns. The material models proposed by Susantha et al. (2001), Sakino et al. (2004), Han et al. (2005), Hatzigeorgiou (2008a, b), Liang (2008), Liang and Fragomeni (2009), and Denavit and Hajjar (2012) are empirical and primarily based on experimental data. The difficulty in utilizing experimental data to develop uniaxial material models is that the contributions from the steel or concrete are generally not directly measured and assumptions are required to extract individual responses (Denavit and Hajjar 2012). The normal practice is to assume an elastic-plastic response with or without strain-hardening for steel. The $\sigma-\varepsilon$ curve of the concrete is derived from the experimental data by deducting the contribution from the steel. After that, an empirical concrete model can be developed based on regression analysis. Although empirical models may give reasonable predictions, they cannot reflect the actual interaction between the steel tube and core concrete because the effects of local buckling and concrete confinement have not been properly considered in the steel model. Furthermore, the accuracy of the empirical models depends on the quality of input information, and the validity is restricted to the test data range for optimizing the model parameters.

A more scientific way to develop $\sigma-\varepsilon$ models for FBE analysis is based on 3D FE modeling, provided that the detailed model has been rigorously validated (Shams and Saadeghvaziri 1999; Varma et al. 2005). Lai and Varma (2016) recently conducted 3D FE analysis of circular CFST columns and found that the axial stress−strain curve of steel has an initial ascending branch followed by a descending branch. The postpeak response of the steel is mainly due to the tensile hoop stresses developing in the steel tube to confine the concrete infill as it reaches its compressive peak stress. The confined concrete, however, may demonstrate strain-softening or strain-hardening behavior depending on the confinement level. For simplicity, however, Lai and Varma (2016) only proposed idealized elastic-perfectly plastic models for both the steel and concrete. Ideally, steel and concrete models should be proposed to represent the actual material responses.

In recent years, high-strength steel and concrete materials have been increasingly used in structures. For example, steel yield

[1]Ph.D. Candidate, Centre for Infrastructure Engineering, Western Sydney Univ., Penrith, NSW 2751, Australia. E-mail: u.katwal@westernsydney.edu.au

[2]Professor, Centre for Infrastructure Engineering, Western Sydney Univ., Penrith, NSW 2751, Australia (corresponding author). E-mail: z.tao@westernsydney.edu.au

[3]Postdoctoral Research Fellow, Centre for Infrastructure Engineering, Western Sydney Univ., Penrith, NSW 2751, Australia. E-mail: k.hassan@westernsydney.edu.au

[4]Professor, School of Civil Engineering, Lanzhou Univ. of Technology, Lanzhou 730050, China. E-mail: wangwd@lut.cn

Note. This manuscript was submitted on October 3, 2016; approved on May 30, 2017; published online on October 4, 2017. Discussion period open until March 4, 2018; separate discussions must be submitted for individual papers. This paper is part of the ***Journal of Structural Engineering***, © ASCE, ISSN 0733-9445.

stress (f_y) of 590 MPa and concrete unconfined strength (f'_c) of 150 MPa have been used in CFST columns in Abeno Harukas, Japan (Liew et al. 2014). Xiong et al. (2017) presented test results of CFST columns filled with concrete of f'_c close to 200 MPa. With the advancements in high-strength materials, thin-walled tubes are more likely to be used in composite columns. To embrace the development of materials, there is a strong need to develop versatile, computationally simple, yet accurate steel and concrete models for the analysis of CFST columns.

This paper utilizes a 3D FE model developed by Tao et al. (2013b) to generate uniaxial effective stress–strain curves for the steel tube and core concrete to cover a wide range of parameters. Based on the numerical data, regression analysis is conducted to propose comprehensive stress–strain models of steel and concrete for FBE modeling.

Numerical Modeling

3D Finite-Element Model

This paper develops the effective stress–strain ($\sigma-\varepsilon$) relationships of steel and concrete in circular CFST columns based on the 3D FE model developed by Tao et al. (2013b), which was verified by a total of 142 full-range load–deformation curves of circular CFST stub columns collected from the literature. Fig. 1(a) shows a typical 3D FE model built in *ABAQUS*, where the steel tube and concrete were simulated by four-node shell elements with reduced integration (S4R) and eight-node brick elements with three translational degrees of freedom at each node (C3D8R), respectively. The mesh size of each discretized element was taken as $D/15$, where D is the overall diameter of the circular tube. In general, the detailed model contains over 4,000 elements for a typical stub column. Because the nonlinear analysis could be conducted within a reasonable computational time, no efforts were made to improve the computational efficiency using a half-symmetry or quarter-symmetry model. The surface-to-surface contact option available in *ABAQUS* was used to model the interaction between the steel tube and concrete. The steel model used by Tao et al. (2013b) is only valid when the yield stress (f_y) is 800 MPa or less. This paper extends the validity range of f_y to 960 MPa. Based on the coupon test results reported by Shi et al. (2012), Qiang et al. (2013), and Shi et al. (2015), the ultimate strength (f_u) is taken as $1.05f_y$ for steel with a f_y between 800 and 960 MPa. More details about the FE modeling are found in Tao et al. (2013b).

Fiber Beam Element Model

The FBE model is an advanced tool in which the member is divided into a number of longitudinal fiber elements [Figs. 1(b and c)]. The geometric characteristics to be defined for a fiber are its area and location with respect to the cross section (Taucer et al. 1991). In FBE modeling of CFST columns, the interaction between the steel tube and concrete core needs to be specifically considered in the input material models to get accurate results. Because of the computational efficiency, FBE models have been commonly used in advanced analysis of frames, where the design process can be simplified because the system strength can be directly assessed from the analysis without the need for calculating the effective length factor or checking the specification of beam-column interaction equations (Zhang and Rasmussen 2013). In particular, FBE models are very suitable for analyzing structures subjected to

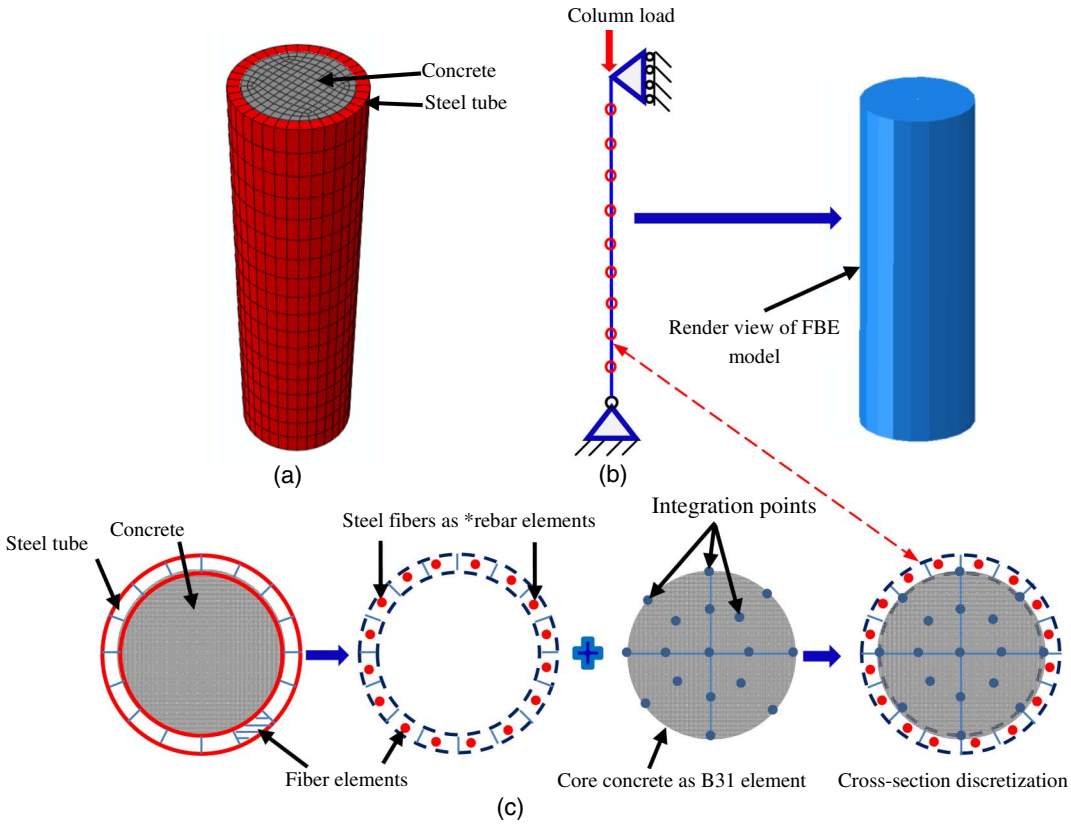

Fig. 1. Typical sketch of FE and FBE models for circular CFST columns: (a) solid FE model; (b) FBE model; (c) discretization of the steel tube and concrete core

extreme events, such as fire, blast, seismic, and other abnormal events.

Assumptions Used in FBE Modeling

In conducting FBE modeling of CFST stub columns, the following assumptions were adopted:

1. A plane section remains plane during deformation;
2. A perfect bond exists between the steel tube and concrete infill;
3. The longitudinal stress of any fiber is only decided by the strain at that point;
4. The effects of concrete creep and shrinkage are not considered; and
5. Steel fracture is also not considered because it typically does not occur until very late in loading histories (Denavit and Hajjar 2012).

Therefore the results of the FBE modeling are only valid before the steel reaches its tensile strain, which is sufficient for the needs of normal analysis.

Procedure for FBE Modeling

To generate the FBE model in *ABAQUS*, the steel tube and concrete core were subdivided into a finite number of longitudinal fibers [Fig. 1(c)]. The concrete was simulated using a two-node linear beam element (B31), which is a first-order three-dimensional Timoshenko element. By changing the number of the material integration points, the number of concrete fibers could be changed accordingly. For the steel tube, the steel fibers were directly defined as material integration points using the *rebar option available in the keywords platform in *ABAQUS* (Wang et al. 2013). The steel and concrete material models were defined through a user material (UMAT) subroutine which was developed using the platform of *Intel Fortran Compiler* and implemented in *ABAQUS* through Microsoft *Visual Studio*.

Sensitivity analysis was conducted to find out the influence of section discretization on the simulation accuracy. For CFST stub columns under axial compression, the effect of the mesh size and section discretization had no obvious influence on the predicted axial load–strain (N–ε) curves. Identical specimens H-58-1 and H-58-2 and specimen CU-070 tested by Sakino and Hayashi (1991) and Huang et al. (2002) were taken as examples [Figs. 2(a and b), respectively]. Almost the same predictions were obtained using different mesh sizes and different numbers of fiber elements. This is understandable because the whole stub column is under axial compression. Similar behavior was observed by Patel et al. (2014) for axially loaded concrete-filled stainless steel short columns. However, section discretization is a prerequisite for fiber element modeling (Patel et al. 2014). This study divided the steel tube into 16 longitudinal fiber elements, and specified 17 longitudinal material integration points for the core concrete. Meanwhile, the CFST column was divided into 10 elements along its length. In specifying the boundary conditions, only vertical displacement at the top end was allowed, whereas all other translational degrees of freedom were restrained for both ends of the CFST column.

Development of Material Models for FBE Modeling

For a CFST column under axial compression, interaction can develop between the steel tube and concrete. Thus the concrete can have increased compressive strength and ductility due to the confinement of the steel tube. Meanwhile, tensile hoop stresses will develop in the steel tube, which reduces its load-carrying capacity in the axial direction (Lai and Varma 2016). During the loading process, the confining stresses change with increasing axial deformation. Furthermore, local buckling of the steel tube might occur during the process, which affects the interaction between the steel tube and concrete. The combined influence of all these factors is very complex and should be properly considered when proposing material models.

To develop simplified material models for the steel tube and concrete in CFST columns, the detailed FE model developed by Tao et al. (2013b) was used to analyze 210 circular CFST stub columns using various parameter combinations. Six yield stress levels were chosen for the steel (f_y = 186, 300, 500, 650, 800, and 960 MPa), whereas five cylinder compressive strength levels were chosen for the concrete (f_c' = 20, 50, 100, 150, and 200 MPa). The diameter:thickness ratio varied at seven levels (D/t = 10, 33, 52, 75, 100, 150, and 220, where t is the thickness of the steel tube). In the analysis, the length:diameter ratio (L/D) was kept constant at 3, so the columns can be classified as stub columns (Tao et al. 2013b). From the simulation, axial stresses of all elements were extracted from the middle section of the CFST column. Then the stresses of all steel elements were averaged to obtain the effective stress (σ) for the steel as a function of the axial strain (ε). A similar procedure was adopted to obtain the effective uniaxial σ–ε relationship for the concrete. Because the averaged σ–ε curves already incorporate the influence of the interaction between the steel tube and concrete, these σ–ε curves can be directly used in FBE modeling. Using the numerical data generated from the 3D FE modeling, regression analysis was conducted to propose suitable steel and concrete material models to represent the effective uniaxial σ–ε relationships.

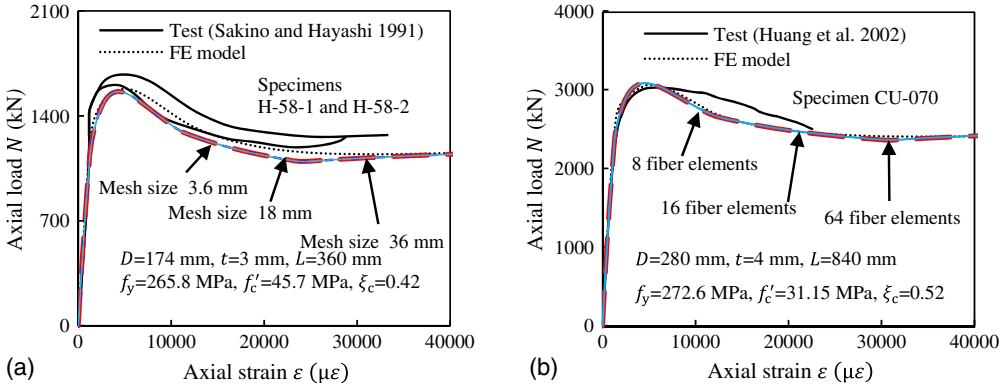

Fig. 2. Influence of mesh size and number of fiber elements of steel tube: (a) influence of mesh size; (b) number of fiber elements

Steel Material Model

Characteristics of Stress–Strain Curves for Steel

In 3D FE modeling, normally only a single σ–ε relationship is required as input for steel, and Tao et al. (2013b) used an elastic-plastic model with strain-hardening, which is also adopted in the present study. Typical CFST stub columns with different confinement factors ($\xi_c = A_s f_y / A_c f_c'$) were analyzed using the 3D FE modeling; Fig. 3(a) compares the obtained effective σ–ε curves of steel. Obviously, these effective σ–ε curves are quite different from the input σ–ε curve. This is because of the development of hoop stresses in the steel tube and possible local buckling of the steel tube. This observation highlights the need to develop a proper effective σ–ε model for steel in FBE modeling.

In general, the effective σ–ε curves of different columns coincide with each other very well in the elastic stage. This can be explained by the weak interaction between the steel tube and concrete in the beginning (Han et al. 2014a; Chacon 2015). However, after reaching the peak stress, the curves differ significantly from each other [Fig. 3(a)]. This is due to the concrete dilation, which strengthens the interaction between the steel and concrete components. The increasing interaction leads to the fast increase of the hoop stress and decrease of the axial stress in the steel tube. Liew and Xiong (2012) discusses this phenomenon further. Fig. 3(a) also shows that the descending speed of a column with a smaller ξ_c is faster than that of the column with a larger ξ_c. The former also has lower residual strength. This is because the concrete dilates faster when the confinement is less significant for the column with a smaller ξ_c. After reaching a critical point [$(\varepsilon_{cr}', f_{cr}')$, where ε_{cr}' and f_{cr}' are the critical strain and stress, respectively], the axial stress increases again because of the strain hardening effect of steel considered in the input model.

There are a few simplified steel σ–ε models available in the literature for the fiber modeling of the steel tubes in CFST columns. Elastic-perfectly plastic σ–ε models with yield stress reduction factors of 0.89 and 0.9 were proposed by Sakino et al. (2004) and Lai and Varma (2016), respectively. Liang and Fragomeni (2009) proposed an idealized linear-rounded-linear σ–ε model with strain hardening for normal steel, and the rounded part of the curve was replaced with a straight line for high-strength steel. Only Denavit and Hajjar (2012) presented a steel model with a softening branch after yielding for circular CFST columns. However, they adopted a constant slope for the descending branch. No existing model can capture all the characteristics of the effective stress-strain curves presented in Fig. 3(a) for steel. Therefore a new model is proposed in the following subsection to fill this research gap.

Proposed Steel Stress–Strain Relationship

The steel σ–ε model used by Tao et al. (2013b) in 3D FE modeling was originally proposed by Tao et al. (2013a) based on statistical analysis of a wide range of σ–ε curves of steel. Because that model cannot be directly used in FBE modeling, as discussed in the previous subsection, suitable modifications should be made to capture the interaction between the steel tube and core concrete. In the present study, the model proposed by Tao et al. (2013a) is revised and expressed for FBE modeling as

$$\sigma = \begin{cases} E_s \varepsilon & 0 \le \varepsilon < \varepsilon_y' \\ f_{cr}' - (f_{cr}' - f_y') \cdot \left(\dfrac{\varepsilon_{cr}' - \varepsilon}{\varepsilon_{cr}' - \varepsilon_y'} \right)^{\psi} & \varepsilon_y' \le \varepsilon < \varepsilon_{cr}' \\ f_u' - (f_u' - f_{cr}') \cdot \left(\dfrac{\varepsilon_u - \varepsilon}{\varepsilon_u - \varepsilon_{cr}'} \right)^{p} & \varepsilon_{cr}' \le \varepsilon < \varepsilon_u \\ f_u' & \varepsilon \ge \varepsilon_u \end{cases} \quad (1)$$

where f_y' = first peak stress of steel in the CFST column; ε_y' ($=f_y'/E_s$) = strain corresponding to f_y'; E_s = Young's modulus of steel, which can be taken as 200 GPa if the value was not reported in a test; ψ and p = strain softening and hardening exponents, respectively; and f_u' = effective stress of steel corresponding to the ultimate strain (ε_u). Tao et al. (2013a) proposed Eq. (2) to determine ε_u of steel. The upper limit for f_y is 800 MPa in the original equation. The following linear equation is proposed to determine ε_u when f_y is between 800 and 960 MPa based on ten coupon test results of S960 steel reported by Shi et al. (2012), Qiang et al. (2013), and Shi et al. (2015):

$$\varepsilon_u = \begin{cases} 100\varepsilon_y & f_y \le 300 \text{ MPa} \\ [100 - 0.15(f_y - 300)]\varepsilon_y & 300 < f_y \le 800 \text{ MPa} \\ [25 - 0.1(f_y - 800)]\varepsilon_y & 800 < f_y \le 960 \text{ MPa} \end{cases} \quad (2)$$

where ε_y = yield strain of steel, taken as f_y/E_s. Fig. 4 shows a schematic view of the simplified σ–ε curves with high, medium, and low ξ_c values. Six parameters (f_y', f_{cr}', ε_{cr}', f_u', ψ, and p) are required to define the σ–ε relationship of steel. Regression analysis was conducted to derive equations for these parameters using the numerical data generated from the 3D FE modeling.

First Peak Stress f_y'

The ratio of f_y'/f_y is an indication of the initial intensity of the interaction between the steel tube and concrete. The stronger the interaction, the higher the hoop stresses developed in the steel tube and the lower the f_y'/f_y ratio. Based on parametric analysis, the ratio of f_y'/f_y is mainly affected by $\varepsilon_y/\varepsilon_{c0}$ and the D/t ratio,

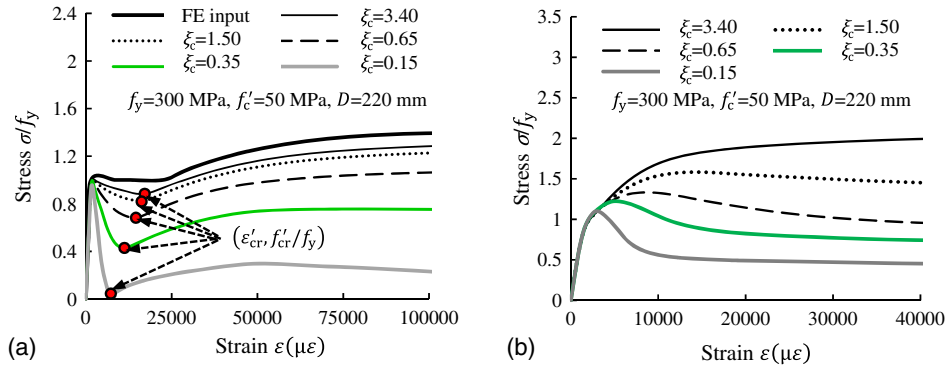

Fig. 3. Effective σ–ε curves of steel and concrete: (a) steel σ–ε curves; (b) concrete σ–ε curves

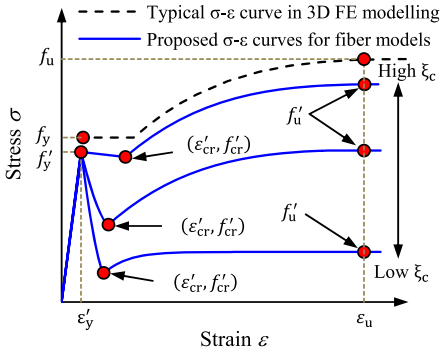

Fig. 4. Proposed steel σ–ε curves for FBE modeling

where ε_{c0} is the strain at peak stress of the corresponding unconfined concrete, and can be determined by (De Nicolo et al. 1994)

$$\varepsilon_{c0} = 0.00076 + \sqrt{(0.626 f'_c - 4.33) \times 10^{-7}} \tag{3}$$

where f'_c is expressed in MPa.

The ratio of f'_y/f_y decreases with increasing $\varepsilon_y/\varepsilon_{c0}$ ratio. This is because a smaller $\varepsilon_y/\varepsilon_{c0}$ ratio represents a relatively slower initiation of the concrete dilation, leading to a weaker initial interaction. Meanwhile, f'_y/f_y decreases with an increase in D/t ratio. When D/t decreases, the concrete is under increased confinement. However, the ratio of the hoop tensile stress to the yield stress of the steel tube decreases, leading to increased f'_y/f_y ratio. Based on regression analysis, Eq. (4) is proposed to determine f'_y/f_y; Fig. 5 demonstrates the prediction accuracy. The coefficient of determination R^2 is 0.81, indicating a reasonably good fit

$$\frac{f'_y}{f_y} = 1.02 - 0.01 \cdot \left(\frac{\varepsilon_y}{\varepsilon_{c0}}\right)^{1.5} \left(\frac{D}{t}\right)^{0.5} \le 1 \tag{4}$$

Critical Stress f'_{cr} and Critical Strain ε'_{cr}

By analyzing the numerical data obtained from FE modeling, it is found that the ratio of the critical stress f'_{cr} to the yield stress f_y is mainly determined by ξ_c. When ξ_c increases to approximately 0.6, f'_{cr}/f_y increases almost linearly to 0.6. Above $\xi_c = 0.6$, f'_{cr}/f_y increases slowly with increasing ξ_c. Eq. (5) is developed to determine f'_{cr}, and Fig. 6 compares the predictions from this equation with the data obtained from FE modeling. The value of R^2 is 0.99 for the proposed equation, which indicates an excellent correlation between the predictions and the numerical data

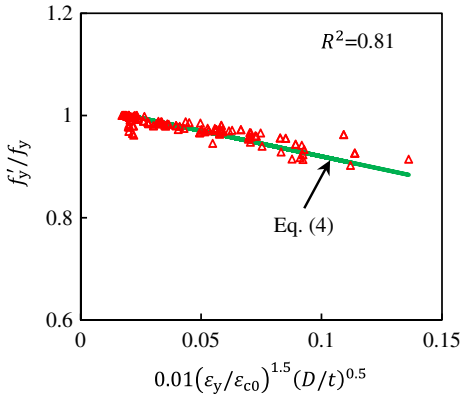

Fig. 5. Verification of proposed equation of f'_y

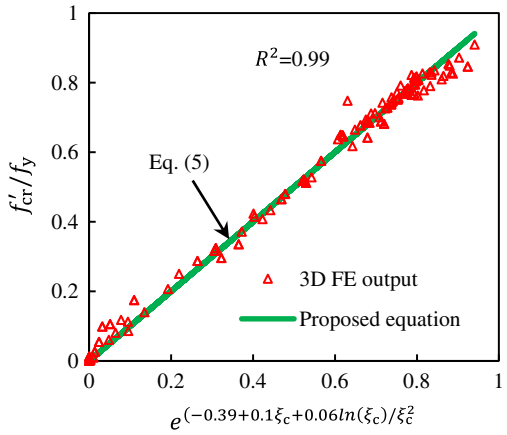

Fig. 6. Verification of proposed equation of f'_{cr}

$$f'_{cr} = f_y \cdot e^{(-0.39+0.1\xi_c+0.06\ln(\xi_c)/\xi_c^2)} > 0 \quad \text{and} \quad \le f'_y \tag{5}$$

The critical strain ε'_{cr} is also mainly dependent on ξ_c. Fig. 3 shows that ε'_{cr} increases with increasing ξ_c. When ξ_c increases, the confinement of concrete is stronger, leading to a slower concrete dilation. Thus the strain-hardening of the steel is delayed. When ξ_c is smaller than 0.5, ε'_{cr} increases almost linearly with the increase of ξ_c. Above $\xi_c = 0.5$, the increase in ε'_{cr} becomes slower. Regression analysis indicates that ε'_{cr} may be expressed as a function of ξ_c only. However, if other terms, such as f_y, f'_c, and D/t are introduced as additional terms, a better model can be produced for ε'_{cr} (Fig. 7), for which the value of R^2 is 0.96. Eq. (6) is proposed to predict ε'_{cr}:

$$\varepsilon'_{cr} = \varepsilon_y \left[28 - 0.07\xi_c - \frac{12}{\xi_c^{0.2}} - 0.13 f_y^{0.75} \left(\frac{t}{D \cdot (f'_c)^{0.7}}\right)^{0.07}\right] \ge \varepsilon_y \quad \text{and} \quad \le \varepsilon_u \tag{6}$$

Stress f'_u

Steel under uniaxial tension can reach its tensile strength f_u corresponding to the ultimate strain ε_u. However, for the steel tube of the CFST column, the obtained effective stress f'_u at ε_u is smaller than f_u because the steel tube has to resist the additional hoop stress in the lateral direction. It is found that factors affecting ε'_{cr} also have similar influence on f'_u. Therefore, similar to Eq. (6), Eq. (7) is proposed to determine f'_u, which has very good agreement ($R^2 = 0.92$) with the data obtained from FE modeling (Fig. 8)

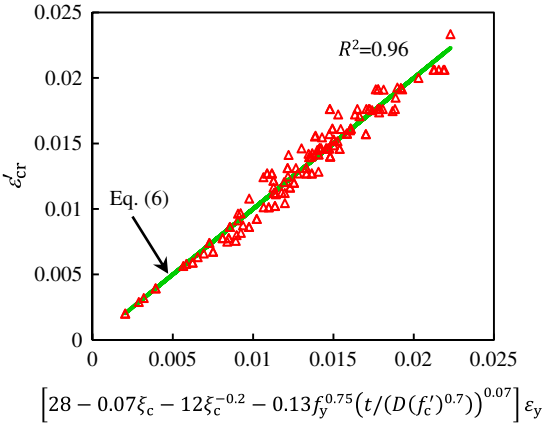

Fig. 7. Verification of proposed equation of ε'_{cr}

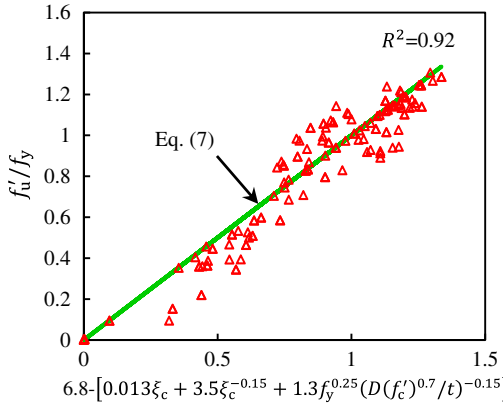

Fig. 8. Verification of proposed equation of f'_u

$$f'_u = f_y\left[6.8 - 0.013\xi_c - \frac{3.5}{\xi_c^{0.15}} - 1.3f_y^{0.25}\left(\frac{t}{D\cdot(f'_c)^{0.7}}\right)^{0.15}\right] > f'_{cr} \quad \text{and} \quad \le f_u \tag{7}$$

Strain Softening Exponent ψ and Strain Hardening Exponent p

Strain softening exponent ψ was calibrated from the FE modeling results. A constant value of 1.5 can be reasonably used to represent ψ (Fig. 9). Although there is some variation, this constant value of 1.5 suggested for ψ is acceptable because it only slightly affects the softening branch of the σ–ε curve.

The strain hardening exponent p is proposed in Eq. (8), which is modified from an equation originally proposed by Tao et al. (2013a). The modification is made by simply replacing the relevant parameters with ε'_{cr}, f'_u, and f'_{cr}, respectively

$$p = E_p\left(\frac{\varepsilon_u - \varepsilon'_{cr}}{f'_u - f'_{cr}}\right) \tag{8}$$

where E_p = initial modulus of elasticity at the onset of strain-hardening, and can be taken as $0.02E_s$.

The proposed steel model can accurately predict the effective σ–ε curve of steel obtained from 3D FE modeling, as shown in Fig. 10(a), where the σ–ε model input into *ABAQUS* is designated as 3D FE input and the obtained effective σ–ε curve is shown as 3D FE output. In this example, the specimen 4LN tested by Tomii et al. (1977) was used.

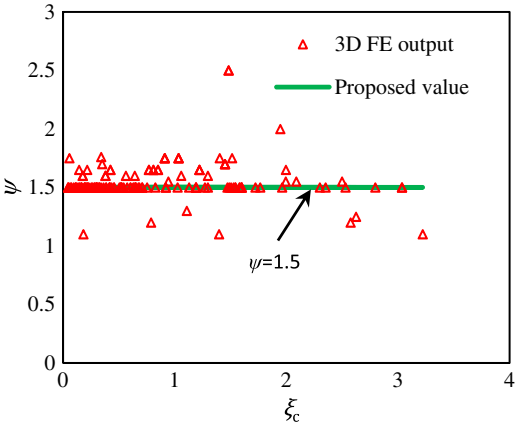

Fig. 9. Verification of proposed value of ψ

Concrete Material Model

Characteristics of Stress–Strain Curves for Concrete

It is well-documented in the literature that the confinement provided by the steel tube can increase the concrete strength and ductility (Han et al. 2014b; Liew and Xiong 2012). However, the concrete confinement is of a passive nature and very difficult to quantify. The confinement factor ξ_c is a comprehensive parameter, which can reasonably reflect the intensity of the concrete confinement (Han et al. 2014b). Based on 3D FE modeling, Fig. 3(b) depicts the effective σ–ε curves of concrete for CFST columns with different ξ_c values. When the confinement is strong, there is a significant improvement in strength and ductility, and no softening branch is available. On the other hand, the improvement in concrete strength and ductility is relatively limited if the confinement is weak.

Lai and Varma (2016) proposed an elastic-perfectly plastic σ–ε model for concrete of circular CFST columns. However, it cannot be used for weakly-confined concrete with a strain-softening branch. In contrast, other empirical concrete models proposed by Susantha et al. (2001), Sakino et al. (2004), and Liang and Fragomeni (2009) normally have a strain-softening response after reaching its peak stress. Because their steel models did not properly consider the strength reduction resulting from the interaction between the steel tube and concrete, the strength reduction of steel has to be incorporated into the concrete models. Thus these empirical concrete models cannot reflect the actual concrete σ–ε response shown in Fig. 3(b). Meanwhile, these existing empirical models are normally only validated by test results of normal CFST columns. With the development of high-strength steel and concrete, there is a need to develop a more versatile concrete model to cover a wider range of parameters.

Proposed Concrete Stress–Strain Relationship

Samani and Attard (2012) proposed a σ–ε model for confined concrete which was verified by extensive test results. They used a single expression to represent both the ascending and descending branches. The model proposed by Samani and Attard (2012) was revised in the present study to represent the effective σ–ε curve of concrete confined by the steel tube, which is expressed by

$$\sigma = \begin{cases} \dfrac{A\cdot X + B\cdot X^2}{1+(A-2)\cdot X+(B+1)\cdot X^2}\cdot f'_{cc} & X\le 1 \text{ or } (X>1 \text{ and } \sigma > f_r) \\ f_r & X>1 \text{ and } \sigma \le f_r \end{cases} \tag{9}$$

where $X = \varepsilon/\varepsilon'_{cc}$, f'_{cc}, and ε'_{cc} are the confined concrete strength and the corresponding strain; f_r = residual stress of concrete (Fig. 11); and A and B = coefficients to determine the shape of the σ–ε curve.

Fig. 11 shows the effective σ–ε curves for weakly confined concrete and strongly confined concrete. To define the full-range curves, five parameters—f'_{cc}, ε'_{cc}, f_r, A, and B—are required. Based on the numerical data generated from the 3D FE modeling, regression analysis was conducted to derive suitable equations for these parameters.

Confined Concrete Strength f'_{cc} and Corresponding Ultimate Strain ε'_{cc}

The parameter f'_{cc} directly reflects the concrete strength increase due to the confinement effect. Parametric analysis indicates that f'_{cc} depends mainly on ξ_c. The ratio of f'_{cc}/f'_c increases with increasing ξ_c. To further improve the prediction accuracy, other terms including f_y, f'_c and D/t ratio are introduced into Eq. (10) to

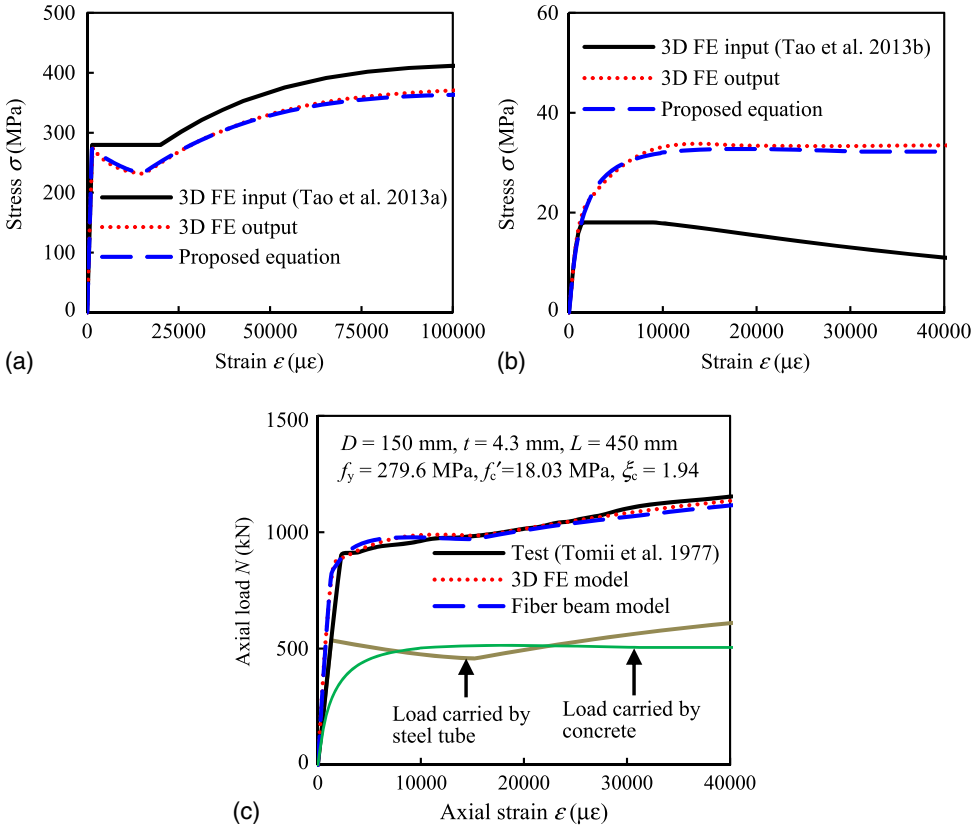

Fig. 10. Validation of steel and concrete material models: (a) comparison of steel models; (b) comparison of concrete models; (c) comparison of predicted and measured N–ε curves

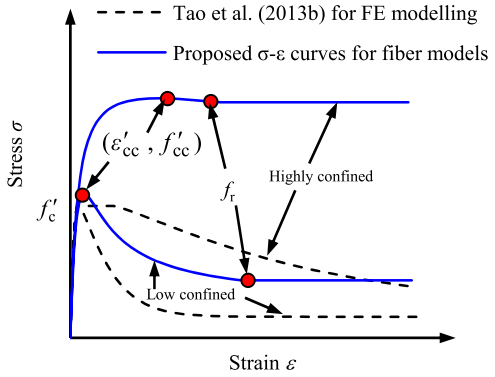

Fig. 11. Proposed σ–ε curves of confined concrete

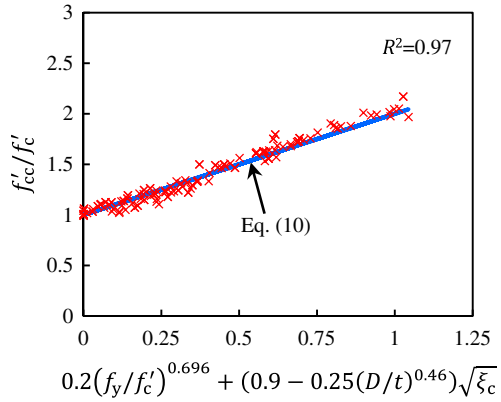

Fig. 12. Verification of proposed equation of f'_{cc}

determine f'_{cc}. Fig. 12 shows that excellent prediction accuracy ($R^2 = 0.97$) was obtained between f'_{cc} calculated from the proposed equation and that obtained from FE modeling

$$\frac{f'_{cc}}{f'_c} = 1 + 0.2 \cdot \left(\frac{f_y}{f'_c}\right)^{0.696} + \left(0.9 - 0.25 \cdot \left(\frac{D}{t}\right)^{0.46}\right) \cdot \sqrt{\xi_c} \geq 1 \quad \text{and} \quad \leq 3 \qquad (10)$$

where f'_c is in MPa.

The strain ε'_{cc} corresponding to f'_{cc} partially reflects the deformation capacity and ductility of a CFST column. Based on the same procedure of regression analysis, Wang et al. (2017) proposed Eq. (11) to predict ε'_{cc}, and this equation is directly adopted in this paper. Wang et al. (2017) limited the maximum value of ε'_{cc} to 0.01 for design purposes. This study removes this limitation

$$\varepsilon'_{cc} = 3{,}000 - 10.4 \cdot f_y^{1.4}(f'_c)^{-1.2}\left[0.73 - 3{,}785.8\left(\frac{D}{t}\right)^{-1.5}\right](\mu\varepsilon) \qquad (11)$$

Residual Concrete Strength f_r

To analyze structures with large deformation, it is necessary to define the residual strength f_r for the confined concrete. Parametrical analysis indicates that the ratio of f_r/f'_{cc} is mainly affected by D/t,

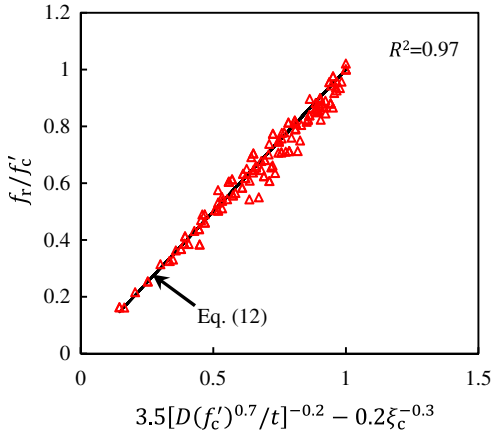

Fig. 13. Verification of proposed equation of f_r

f_c', and ξ_c. It was found that f_r/f_{cc}' decreases with increasing D/t or f_c', and increases with an increase in ξ_c. Regression analysis was conducted, and Eq. (12) is proposed to predict f_r/f_{cc}', which is a function of D/t, f_c', and ξ_c. The correlation ($R^2 = 0.97$) between the proposed equation and the simulation results is very close (Fig. 13)

$$f_r = f_{cc}'\left[3.5 \cdot \left(\frac{t}{D \cdot (f_c')^{0.7}}\right)^{0.2} - \frac{0.2}{\xi_c^{0.3}}\right] \le f_{cc}' \tag{12}$$

where f_c' is in MPa.

Coefficients *A* and *B*

The coefficient A determines the shape of the ascending part, and Samani and Attard (2012) suggested $A = E_c\varepsilon_{cc}'/f_{cc}'$, where E_c is the modulus of elasticity of unconfined concrete and can be taken as $4{,}700\sqrt{f_c'}$ according to ACI 318 (ACI 2011), where f_c' is in MPa. However, the proposed equation for A by Samani and Attard (2012) is for actively confined concrete, which cannot be directly used for CFST columns. The concrete inside a CFST column is passively confined, and the direct use of the coefficient A leads to the underestimation of the initial stiffness of the CFST column. Therefore a correction factor α_1 ranging from 1 to 1.3 is introduced into Eq. (13) to determine the coefficient A

$$A = \alpha_1 \frac{E_c\varepsilon_{cc}'}{f_{cc}'} \tag{13}$$

Parametric analysis indicates that α_1 has a strong correlation with ξ_c. Based on numerical tests, suitable values of α_1 were determined for CFST columns with different ξ_c values. A regression analysis was conducted and Eq. (14) is proposed accordingly to determine α_1 as follows:

$$\alpha_1 = 1 + 0.25 \cdot \xi_c^{(0.05+0.25/\xi_c)} \tag{14}$$

The coefficient B controls the shape of the descending part. The smaller the coefficient B, the steeper the descending curve. The coefficient B increases with increasing ξ_c or decreasing f_c'. The value of B normally ranges from -0.75 to 2. For normal strength concrete with reasonably good confinement, B will be positive. However, B becomes negative for weakly confined concrete or high-strength concrete. Based on numerical tests, suitable values of B were determined for CFST columns with different combinations of ξ_c and f_c'. Based on regression analysis, Eq. (15) is proposed to determine the coefficient B as follows:

$$B = 2.15 - 2.05e^{-\xi_c} - 0.0076f_c' \ge -0.75 \tag{15}$$

The proposed concrete model can accurately predict the effective σ–ε curve of concrete obtained from 3D FE modeling [Fig. 10(b)]. As demonstrated by this example, all characteristics of the effective σ–ε curve of concrete are well captured by the proposed model.

Verification of Fiber Beam Element Modeling

The axial load–axial strain (N–ε) curves of 150 circular CFST stub columns collected from 22 sources were used to verify the proposed FBE model. The majority of the test data was collected by Tao et al. (2013b) for developing the 3D FE model. In addition, some newly reported test data were collected and assembled in the database (Table 1). The majority of the test data are from extensively cited references. The ranges of parameters for the test specimens are $f_y = 186$–853 MPa, $f_c' = 18$–193 MPa, $D = 60$–450 mm, $D/t = 17$–221, and $L/D = 1.8$–4.8. These parameters cover sufficiently wide practical ranges (Table 1).

The predicted ultimate strengths (N_{uc}) from the FBE modeling were compared with the measured ultimate strengths (N_{ue}). Following the definition by Tao et al. (2013b), the ultimate strength in this paper is defined as the peak load if the N–ε curve has a softening branch and the strain corresponding to the peak load is less than 0.01; otherwise it is defined as the load at a strain of 0.01. Fig. 14(a) compares N_{uc}/N_{ue} with respect to ξ_c for all 150 columns; the mean value (μ) and standard deviation (SD) were 0.985 and 0.067, respectively. Meanwhile, the ultimate strengths (N_{uFE}) were also predicted using the 3D FE modeling. Fig. 14(b) compares N_{uFE}/N_{ue} with respect to ξ_c; the obtained μ and SD were 0.992 and 0.064, respectively. Comparable results were obtained from the FBE modeling and the detailed modeling in terms of ultimate strength. In general, the predictions from the FBE modeling were slightly more conservative than the 3D FE predictions, but had similar precision.

Figs. 15(a and b) show the effects of concrete strength and steel yield stress on the prediction accuracy of ultimate strength, respectively. In this paper, concrete with f_c' less than 60 MPa is considered as normal strength concrete (NSC). If f_c' is between 60 and 120 MPa, the concrete is referred to as high-strength concrete (HSC). Concrete with f_c' higher than 120 MPa is considered as ultra-high strength concrete (UHSC). Similarly, steel with f_y less than 460 MPa is considered as normal strength steel (NSS). Otherwise, it is grouped into high strength steel (HSS). The comparison in Fig. 15 indicates that the prediction accuracy of the ultimate strength using the FBE modeling is not obviously affected by f_c' or f_y.

The predictions of the N–ε curves of normal CFST columns from the FBE modeling also agree with the test results and the 3D FE modeling very well. This is seen in Figs. 10(c) and 16, which take specimens 4LN and 3HN tested by Tomii et al. (1977) and C2 tested by Schneider (1998) as examples. The load carried by the steel tube or concrete can be determined by simply multiplying the effective stress of the steel or concrete by the cross-sectional area of the corresponding component. When the load is mainly carried by the steel tube (C2) or it is almost evenly shared by the steel tube and the concrete, the composite column usually does not have a postpeak softening response. In contrast, it usually demonstrates a softening response after the peak load if the concrete carries the majority of the load.

The FBE model can also be successfully used to predict N–ε curves of CFST columns with HSC. Fig. 17 demonstrates this

Table 1. Summary of Test Data for Circular CFST Stub Columns

Number of specimens	D (mm)	t (mm)	ξ_c	D/t	L/D	f_y (MPa)	f_c' (MPa)	Source
7	76–153	1.7–4.1	1.6–2.6	30–48	2.0	363–605	21–34	Gardener and Jacobson (1967)
1	169	2.6	0.563	65	1.8	317	37	Gardener (1968)
23	150	2.0–4.3	0.65–1.6	35–75	3.0	280–336	18–29	Tomii et al. (1977)
12	174–179	3.0–9.0	0.4–3.1	20–58	2.0	248–283	22–46	Sakino and Hayashi (1991)
2	190	1.15	0.05	165	3.5	202.8	110.3	O'Shea and Bridge (1994)
10	165–190	0.9–2.8	0.05–0.54	59–221	3.5	186–363	41–80	O'Shea and Bridge (1998)
2	141	3.0–6.5	0.92–2.8	22–47	4.3	285–313	24–28	Schneider (1998)
12	108–133	1.0–4.7	0.07–0.71	24–125	3.5	232–358	92–106	Tan et al. (1999)
6	102–319	3.2–10.3	0.92–2.5	31–32	3.0	334–452	23–52	Yamamoto et al. (2000)
3	200–300	2.0–5.0	0.34–1.1	40–150	3.0	266–342	27–31	Huang et al. (2002)
2	100–200	3.0	0.385	33–67	3.0	304	50	Han and Yao (2004)
7	114–115	3.8–5.0	0.58–2.0	23–30	2.6	343–365	26–95	Giakoumelis and Lam (2004)
5	108–450	3.0–6.5	0.64–3.22	17–52	3.0	308–853	41–85	Sakino et al. (2004)
22	60–250	1.9–2	0.12–0.52	30–134	3.0	282–404	75–80	Han et al. (2005)
8	89–113	2.7–2.9	1.3–1.7	33–39	3–3.8	360	28–33	Gupta et al. (2007)
2	165	2.7	0.36–0.50	61	3.1	350	48–67	Yu et al. (2007)
4	114.3	3.35	0.35–1.13	34	3.0	287	33–106	de Oliveira et al. (2009)
1	360	6	1.11	60	4.8	498	31.5	Lee et al. (2011)
16	114–219	3.6–10	0.19–1.5	18–44	2.2–2.7	300–428	54–193	Xiong et al. (2017)
2	76.2	3–3.3	0.34–0.42	23–25	3.9	278–316	145	Guler et al. (2013)
2	114.3	4.0–5.9	0.42–0.67	19–28	3.5	306–314	115	Guler et al. (2014)
1	160	3.8	0.83	42	3.0	409	51	Han et al. (2014a)

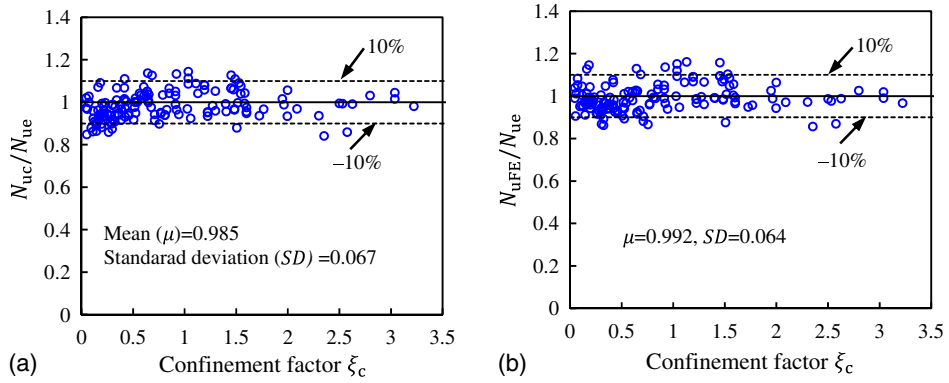

Fig. 14. Comparison of N_{ue} with N_{uc} and N_{uFE} with respect to confinement factor: (a) comparison of N_{uc} and N_{ue}; (b) comparison of N_{uFE} and N_{ue}

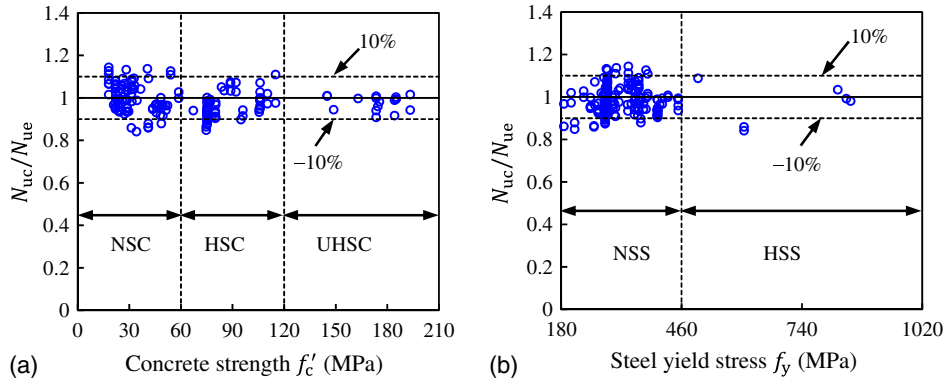

Fig. 15. Comparison of N_{uc} and N_{ue} with respect to material strength: (a) concrete strength (f_c'); (b) steel yield stress (f_y)

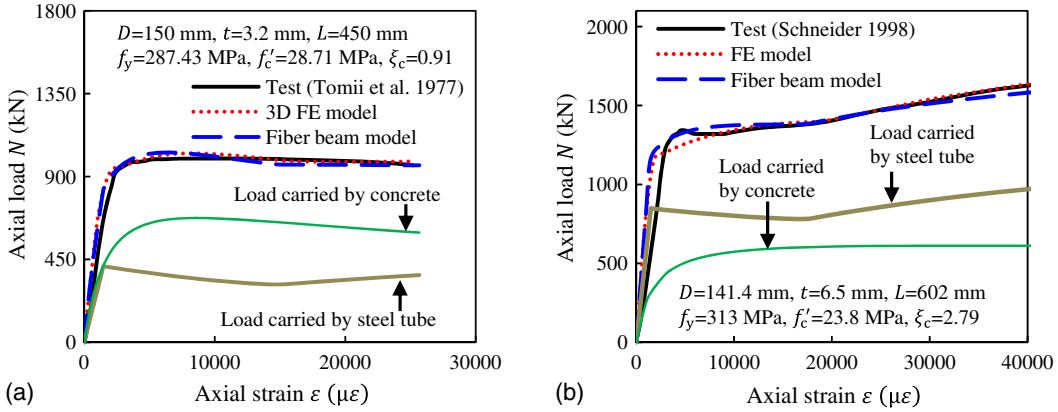

Fig. 16. Comparison of predicted and measured N–ε curves for columns with normal materials: (a) specimen 3HN; (b) specimen C2

for specimens S12CS80A and C-100-3D tested by O'Shea and Bridge (1998) and de Oliveira et al. (2009), respectively. The predicted N–ε curves agree very well with the experimental curves and those predicted by the 3D FE modeling. The FBE model was also used to simulate CFST columns with UHSC concrete. Compared with NSC or HSC, UHSC is more brittle under compression and demonstrates an almost linear σ–ε curve even with confinement from the steel tube. Accordingly, a steep drop in the load–axial shortening curves was observed for UHSC filled tubes immediately after the peak load (Liew et al. 2014). This feature was considered when proposing the concrete model for FBE modeling. Therefore the steep drop in N–ε curves for columns with UHSC is successfully captured in the FBE modeling, as seen in Fig. 18 for the two typical specimens C15 and C14 reported by Xiong et al. (2017). However, the 3D FE model does not accurately capture this behavior.

There are only a few load–deformation curves reported in the literature for circular CFST stub columns with HSS steel. For these

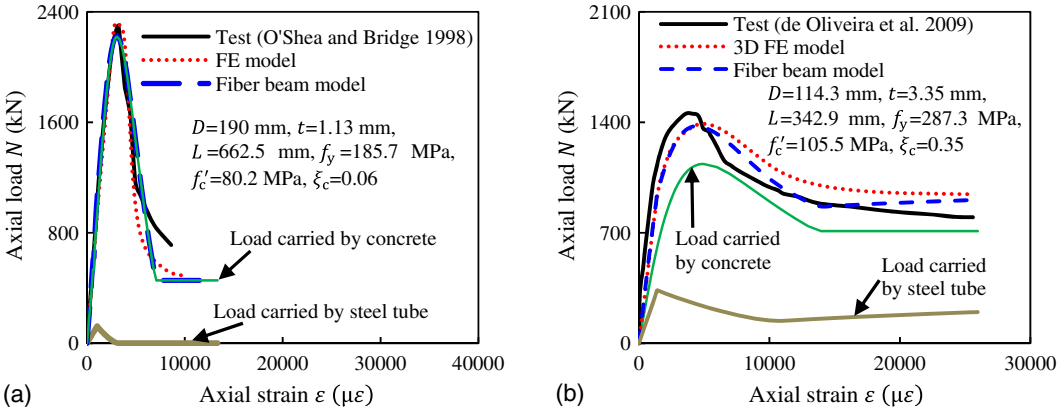

Fig. 17. Comparison of predicted and measured N–ε curves for columns with HSC: (a) specimen S12CS80A; (b) specimen C-100-3D

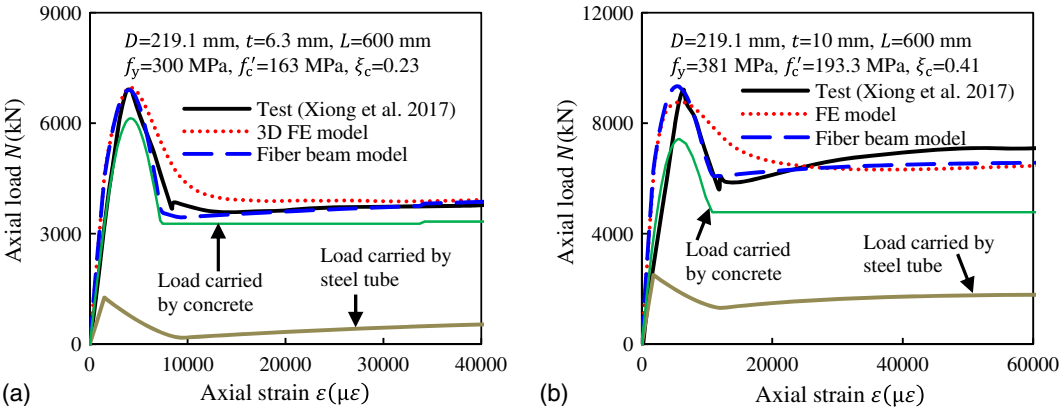

Fig. 18. Comparison of predicted and measured N–ε curves for columns with UHSC: (a) specimen C15; (b) specimen C14

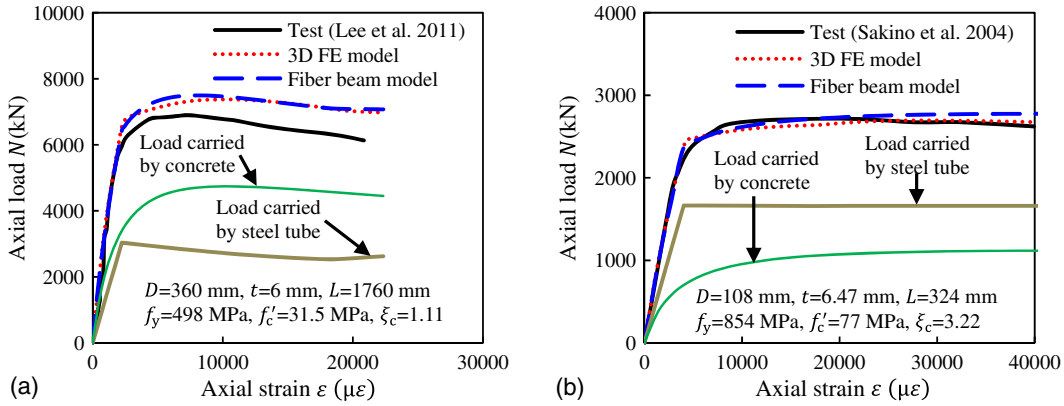

Fig. 19. Comparison of predicted and measured N–ε curves for columns with high-strength steel: (a) specimen 049C36_30; (b) specimen CC8-A-8

columns, very good predictions by the FBE modeling are also obtained as shown in Fig. 19, which takes specimen 049C36_30 tested by Lee et al. (2011) and specimen CC8-A-8 tested by Sakino et al. (2004) as examples.

The proposed FBE model can also be used for concrete-filled thin-walled tubes, or stocky CFST columns with small D/t ratios. Figs. 17(a) and 18(b) show the prediction accuracy for specimen S12CS80A with a tube thickness 1.13 mm and specimen S2-2-4 with a tube thickness of 10 mm, respectively.

The proposed equations in this paper can be directly utilized to calculate the load–deformation curves of circular CFST stub columns using simple spreadsheet software. This can help design engineers to conduct preliminary design of CFST columns.

Concluding Remarks

This paper developed a fiber beam element model for axially loaded circular concrete-filled steel stub columns to achieve a high computational efficiency. Effective steel and concrete stress–strain models were proposed based on detailed finite element modeling. The proposed stress–strain curves for steel implicitly consider the interaction between the steel tube and concrete, possible local buckling of the steel tube, and strain-hardening of the steel material. Meanwhile, the concrete model considers the increase in strength and ductility resulting from the concrete confinement.

The proposed material models were implemented in simplified fiber beam element modeling and the predictions were verified by 3D FE modeling and a large amount of test data collected from the literature. The simplified numerical model proposed in this paper covers a wide range of parameters: diameter:thickness ratio (D/t = 10–220), yield stress (f_y = 186–960 MPa), and concrete cylinder compressive strength (f'_c = 20–200 MPa). The strength increase or degradation of a CFST column after reaching its ultimate strength can be automatically captured in the simulation.

The current research is limited to axially loaded circular CFST stub columns. Further research is required to propose a similar model for rectangular columns because of the difference in section stability and concrete confinement between the two types of columns. Further research is also required to determine if the proposed steel and concrete models can be used in the simulation of slender CFST columns or columns under eccentric loading. The efficiency of the fiber beam element modeling was well demonstrated by Wu et al. (2006) in analyzing the Second Saikai Bridge, with a main span of 240 m. Further research should be conducted to incorporate the proposed material models in FBE modeling of composite frames with CFST columns.

Acknowledgments

This study is supported by Western Sydney University under the International Postgraduate Research Scholarship scheme. This support is gratefully acknowledged.

References

ABAQUS version 6.12 [Computer software]. Dassault Systmes, Providence, RI.

ACI. (2011). *Building code requirements for structural concrete (ACI 318-11) and commentary*, Farmington Hills, MI.

Chacon, R. (2015). "Circular concrete-filled tubular columns: State of the art oriented to the vulnerability assessment." *Open Civ. Eng. J.*, 9(S1), 249–259.

Denavit, M. D., and Hajjar, J. F. (2012). "Nonlinear seismic analysis of circular concrete-filled steel tube members and frames." *J. Struct. Eng.*, 10.1061/(ASCE)ST.1943-541X.0000544, 1089–1098.

De Nicolo, B., Pani, L., and Pozzo, E. (1994). "Strain of concrete at peak compressive stress for a wide range of compressive strengths." *Mater. Struct.*, 27(4), 206–210.

de Oliveira, W. L. A., de Nardin, S., de Cresce El Debs, A. L. H., and El Debs, M. K. (2009). "Influence of concrete strength and length/diameter on the axial capacity of CFT columns." *J. Constr. Steel Res.*, 65(12), 2103–2110.

Gardener, N. J. (1968). "Use of spiral welded steel tubes in pipe columns." *J. Am. Concr. Ins.*, 65(11), 937–942.

Gardener, N. J., and Jacobson, R. (1967). "Structural behavior of concrete filled steel tubes." *ACI J.*, 64(7), 404–413.

Giakoumelis, G., and Lam, D. (2004). "Axial capacity of circular concrete-filled tube columns." *J. Constr. Steel Res.*, 60(7), 1049–1068.

Guler, S., Copur, A., and Aydogan, M. (2013). "Axial capacity and ductility of circular UHPC-filled steel tube columns." *Mag. Concr. Res.*, 65(15), 898–905.

Guler, S., Copur, A., and Aydogan, M. (2014). "A comparative study on square and circular high strength concrete-filled steel tube columns." *Adv. Steel Constr.*, 10(2), 234–247.

Gupta, P. K., Sarda, S. M., and Kumar, M. S. (2007). "Experimental and computational study of concrete filled steel tubular columns under axial loads." *J. Constr. Steel Res.*, 63(2), 182–193.

Han, L. H., Hou, C. C., and Wang, Q. L. (2014a). "Behavior of circular CFST stub columns under sustained load and chloride corrosion." *J. Constr. Steel Res.*, 103(1), 23–36.

Han, L. H., Li, W., and Bjorhovde, R. (2014b). "Developments and advanced applications of concrete-filled steel tubular (CFST) structures: Members." *J. Constr. Steel Res.*, 100(9), 211–228.

Han, L. H., and Yao, G. H. (2004). "Experimental behavior of thin-walled hollow structural steel (HSS) columns filled with self-consolidating concrete (SCC)." *Thin-Walled Struct.*, 42(9), 1357–1377.

Han, L. H., Yao, G. H., and Zhao, X. L. (2005). "Tests and calculations for hollow structural steel (HSS) stub columns filled with self-consolidating concrete (SCC)." *J. Constr. Steel Res.*, 61(9), 1241–1269.
Hatzigeorgiou, G. D. (2008a). "Numerical model for the behavior and capacity of circular CFT columns. Part I: Theory." *Eng. Struct.*, 30(6), 1573–1578.
Hatzigeorgiou, G. D. (2008b). "Numerical model for the behavior and capacity of circular CFT columns. Part II: Verification and extension." *Eng. Struct.*, 30(6), 1579–1589.
Huang, C. S., et al. (2002). "Axial load behavior of stiffened concrete-filled steel columns." *J. Struct. Eng.*, 10.1061/(ASCE)0733-9445(2002)128:9(1222), 1222–1230.
Intel Fortran Compiler version 11.1 [Computer software]. Intel, Santa Clara, CA.
Lai, Z., and Varma, A. H. (2016). "Effective stress-strain relationships for analysis of noncompact and slender filled composite (CFT) members." *Eng. Struct.*, 124(10), 457–472.
Lee, S. H., Uy, B., Kim, S. H., Choi, Y. H., and Choi, S. M. (2011). "Behavior of high-strength circular concrete-filled steel tubular (CFST) column under eccentric loading." *J. Constr. Steel Res.*, 67(1), 1–13.
Liang, Q. Q. (2008). "Nonlinear analysis of short concrete-filled steel tubular beam-columns under axial load and biaxial bending." *J. Constr. Steel Res.*, 64(3), 295–304.
Liang, Q. Q., and Fragomeni, S. (2009). "Nonlinear analysis of circular concrete-filled steel tubular short columns under axial loading." *J. Constr. Steel Res.*, 65(12), 2186–2196.
Liew, J. Y. R., and Xiong, D. X. (2012). "Ultra-high strength concrete filled composite columns for multi-storey building construction." *Adv. Struct. Eng.*, 15(9), 1487–1503.
Liew, J. Y. R., Xiong, M. X., and Xiong, D. X. (2014). "Design of high strength concrete filled tubular columns for tall buildings." *Int. J. High Rise Build.*, 3(3), 215–221.
O'Shea, M. D., and Bridge, R. Q. (1994). "Tests of thin-walled concrete-filled steel tubes." *Proc., 12th Int. Specialty Conf. on Cold-Formed Steel Structure*, American Iron and Steel Institute, Washington, DC, 399–419.
O'Shea, M. D., and Bridge, R. Q. (1998). "Tests on circular thin-walled steel tubes filled with medium and high strength concrete." *Aust. Civ. Eng. Trans.*, 40, 15–27.
Patel, V. I., Liang, Q. Q., and Hadi, M. N. S. (2014). "Nonlinear analysis of axially loaded circular concrete-filled stainless steel tubular short columns." *J. Constr. Steel Res.*, 101(10), 9–18.
Qiang, X., Bijlaard, F. S. K., and Kolstein, H. (2013). "Post-fire performance of very high strength steel S960." *J. Constr. Steel Res.*, 80(1), 235–242.
Sakino, K., and Hayashi, H. (1991). "Behavior of concrete filled steel tubular stub columns under concentric loading." *Proc., 3rd Int. Conf. on Steel-Concrete Composite Structure*, Association for International Cooperation and Research in Steel-Concrete Composite Structures, Harbin, China, 25–30.
Sakino, K., Nakahara, H., Morino, S., and Nishiyama, I. (2004). "Behavior of centrally loaded concrete-filled steel-tube short columns." *J. Struct. Eng.*, 10.1061/(ASCE)0733-9445(2004)130:2(180), 180–188.
Samani, A. K., and Attard, M. M. (2012). "A stress-strain model for uniaxial and confined concrete under compression." *Eng. Struct.*, 41(8), 335–349.
Schneider, S. P. (1998). "Axially loaded concrete-filled steel tubes." *J. Struct. Eng.*, 10.1061/(ASCE)0733-9445(1998)124:10(1125), 1125–1138.
Shams, M., and Saadeghvaziri, M. A. (1999). "Nonlinear response of concrete-filled steel tubular columns under axial loading." *ACI Struct. J.*, 96(6), 1009–1019.
Shi, G., Ban, H., and Bijlaard, F. S. K. (2012). "Tests and numerical study of ultra-high strength steel columns with end restraints." *J. Constr. Steel Res.*, 70(3), 236–247.
Shi, G., Zhou, W., and Lin, C. (2015). "Experimental investigation on the local buckling behavior of 960 MPa high strength steel welded section stub columns." *Adv. Struct. Eng.*, 18(3), 423–437.
Susantha, K. A. S., Ge, H., and Usami, T. (2001). "Uniaxial stress-strain relationship of concrete confined by various shaped steel tubes." *Eng. Struct.*, 23(10), 1331–1347.
Tan, K. F., Pu, X. C., and Cai, S. H. (1999). "Study on mechanical properties of extra-strength concrete encased in steel tubes." *J. Build. Struct.*, 20(1), 10–15.
Tao, Z., Wang, X. Q., and Uy, B. (2013a). "Stress-strain curves of structural and reinforcing steels after exposure to elevated temperatures." *J. Mater. Civ. Eng.*, 10.1061/(ASCE)MT.1943-5533.0000676, 1306–1316.
Tao, Z., Wang, Z. B., and Yu, Q. (2013b). "Finite element modelling of concrete-filled steel stub columns under axial compression." *J. Constr. Steel Res.*, 89(10), 121–131.
Taucer, F. F., Spacone, E., and Fillippou, F. C. (1991). "A fiber beam column element for seismic response analysis of reinforced concrete structures." *Rep. No. UCB/EERC-91/17*, Earthquake Engineering Research Center, College of Engineering, Univ. of California, Berkeley, CA.
Tomii, M., Yoshimura, K., and Morishita, Y. (1977). "Experimental studies on concrete filled steel tubular stub columns under concentric loading." *Proc., Int. Colloquium on Stability of Structure under Static and Dynamic Loads*, Structural Stability Research Council, Chicago, 718–741.
Varma, A. H., Sause, R., Ricles, J. M., and Li, Q. (2005). "Development and validation of fiber model for high-strength square concrete-filled steel tube beam-columns." *ACI Struct. J.*, 102(1), 73–84.
Wang, Y. H., Nie, J. G., and Cai, C. S. (2013). "Numerical modeling on concrete structures and steel-concrete composite frame structures." *Composites Part B Eng.*, 51(8), 58–67.
Wang, Z. B., Tao, Z., Han, L. H., Uy, B., Lam, D., and Kang, W. H. (2017). "Strength, stiffness and ductility of concrete-filled steel columns under axial compression." *Eng. Struct.*, 135(3), 209–221.
Wu, Q., Yoshimura, M., Takahashi, K., Nakamura, S., and Nakamura, T. (2006). "Nonlinear seismic properties of the Second Saikai Bridge: A concrete filled tubular (CFT) arch bridge." *Eng. Struct.*, 28(2), 163–182.
Xiong, M. X., Xiong, D. X., and Liew, J. Y. R. (2017). "Axial performance of short concrete filled steel tubes with high- and ultra-high-strength materials." *Eng. Struct.*, 136(4), 494–510.
Yamamoto, T., Kawaguchi, J., and Morino, S. (2000). "Experimental study of scale effects on the compressive behavior of short concrete-filled steel tube columns." *Proc., United Engineering Foundation Conf. on Composite Construction in Steel and Concrete IV (AICE)*, United Engineering Foundation, Philadelphia, 879–891.
Yu, Z. W., Ding, F. X., and Cai, C. S. (2007). "Experimental behavior of circular concrete-filled steel tube stub columns." *J. Constr. Steel Res.*, 63(2), 165–174.
Zhang, H., and Rasmussen, K. J. R. (2013). "System-based design for steel scaffold structures using advanced analysis." *J. Constr. Steel Res.*, 89(10), 1–8.